Environ. Sci. Technol. **2001**, *35,* 4515−4521

XAS Studies of Ni and Zn Sorbed to Hydrous Manganese Oxide

PARAS TRIVEDI,† LISA AXE,*,† AND TREVOR A. TYSON‡

Department of Civil and Environmental Engineering and Department of Physics, New Jersey Institute of Technology, Newark, New Jersey 07102

Adsorption mechanisms of Zn^{2+} and Ni^{2+} on hydrous manganese oxide (HMO) were investigated using XAS. Analyses reveal that both metal ions retain their primary hydration shell when sorbed to HMO, which is consistent with physical sorption. These local structures are invariant of pH (3.0−7.0) and adsorbate loading (10^{-4} − 10^{-2} mol (g of HMO)$^{-1}$), suggesting one average type of adsorption mechanism. In addition to the first shell, a second shell was observed with 6−8 O atoms at 3.34 Å for Ni and 8−10 O atoms at 3.49 Å for Zn. The lack of Ni or Zn contributions in the second shell eliminates the possibility of surface precipitation or polymerization. Likewise, the absence of Mn atoms in the second shell suggests outer-sphere adsorption. Interestingly, the local structure of Ni and Zn sorbed to HMO did not change with reaction time when as much as 90% of the sorbed contribution was due to the slow sorption process, thus supporting intraparticle diffusion as the rate-limiting mechanism. This result demonstrates that adsorption sites located along the micropore walls of HMO are similar to ones located on the external surface. Overall, metals from the same group in the Periodic Table appear to form similar adsorption complexes with HMO.

Introduction

Manganese oxides are ubiquitous in aquatic environments as discrete particles and as coatings on other minerals (*1*−*4*). Most manganese oxides are typically amorphous consisting of a 3-D framework of randomly distributed edge- and corner-sharing MnO_2 octahedra (*4*−*7*). Hydrated manganese oxides (HMO) have much larger adsorption capacities than iron oxides (*8*−*12*). These oxides play an important role in the oxidation of toxic metals such as Cr(III) to Cr(VI) (*13*), As(III) to As(V) (*14*), and Se(IV) to Se(VI) (*15*). Thermodynamically, Ni and Zn ions have been found to physically sorb to HMO (*12, 16*). Kinetic studies reveal that intraparticle diffusion is the rate-limiting mechanism for metal sorption to HMO, wherein as much as 90% of the adsorption sites are located along the micropore walls of this oxide (*11, 12, 16*). To complement these macroscopic observations and to better understand sorption mechanisms of environmentally relevant metals such as Zn and Ni, spectroscopic studies have been conducted.

X-ray absorption spectroscopy (XAS) is an important tool in environmental research for assessing the nearest neighbors of a metal in situ and under dilute concentrations. XAS has proven to be useful in discerning sorption mechanisms such as inner-sphere complexation (*17*−*31*), outer-sphere complexation (physical sorption) (*23, 24, 32*−*35*), surface precipitation, redox reactions, and formation of mixed oxides. Interestingly, through XAS, studies have revealed surface oxidation of metal ions at the manganese oxide interface: Cr(III) oxidation to Cr(IV) (*18, 36*) and Co(II)EDTA^{2-} to Co(III)EDTA^{-} (*37*). Likewise substantial evidence supports intraparticle diffusion as the rate-limiting mechanism in sorption to microporous oxides: As(V) sorption to ferrihydrite (*38*), Cd and Se(IV) to alumina (*39*), Sr sorption to HFO (*32*) and HMO (*33*), and Cu and Pb sorption to ferrihydrite (*31*).

Sparks and co-workers (*40*−*44*) have found from extensive kinetic studies that, under alkaline conditions, Ni coprecipitates with Al to form a Ni−Al layered double hydroxide (LDH) upon sorption to clays and other minerals including pyrophyllite, gibbsite, montmorillonite, talc, silica, and pyrophyllite−montmorillonite mixtures. In such precipitates, the second shell is generally composed of Ni and Al atoms with Ni/Al coordination ratios ranging from 1 to 3 depending upon the initial conditions (*40*−*44*). Similarly, XAFS studies of Zn sorption to pyrophyllite revealed the formation of a Zn−Al LDH in which crystalline stability increased with aging (*45*). Interestingly, Zn sorption to metal oxides ranges from physical sorption with amorphous oxides (*24*) to chemisorption with crystalline oxides (*23, 24, 46, 47*). However, there is a need to elucidate the sorption mechanisms of Ni and Zn to HMO, a prevalent oxide found in soils and sediments.

Hence, this research is focused on investigating the sorption complexes of Ni and Zn ions with HMO as a function of pH, adsorbate loading, and reaction time. This work will aid in modeling contaminant mobility and bioavailability in subsurface systems rich in amorphous manganese oxides.

Experimental Methods and Analyses

HMO was prepared by slow titration of $Mn(NO_3)_2$ with alkaline $NaMnO_4$ in the molar ratio of 3:2. The solution was mixed for 3 h under a turbulent hydraulic regime ($Re > 3 \times 10^5$) (*11*). Prior to adsorption studies, HMO was centrifuged, washed, and redispersed in Millipore-Q water at 0.015 ionic strength, pH 7, and 25 °C for 24 h. The characteristics and properties of this HMO have been discussed previously (*11*).

Adsorption samples were prepared at pH 7 and 25 °C for the following sorption densities: 1×10^{-4}, 1×10^{-3}, and 1×10^{-2} mol of Zn (g of HMO)$^{-1}$. The distribution analyses of these samples are in agreement with the previous isotherm studies (*12*) where a linear relationship was observed between the sorbed and the bulk aqueous concentrations. To understand the sorption mechanism as a function of pH, samples with a loading of 1×10^{-2} mol of Zn (g of HMO)$^{-1}$ were also prepared at pH 3.5 and pH 5.0. Additionally, in studying intraparticle diffusion, to test whether sorption sites located along the micropore walls are similar to those on the external surface, a 32-day-old sample was also studied. Consistent with the previous macroscopic work (*12*), the sorption density of this sample was 4×10^{-3} mol of Zn (g of HMO)$^{-1}$, of which approximately 33% are located internally.

Ni adsorption to HMO was synthesized at pH 5 and pH 7 at 25 °C for the following sorption densities: 1×10^{-3} and 1×10^{-2} mol of Ni (g of HMO)$^{-1}$; adsorption analyses of these samples are consistent with the isotherm studies reported previously (*16*). To better understand the kinetics of Ni sorption to HMO, XAS samples were prepared from long-term studies maintained at pH 7 and 25 °C after contact times of 20 and 110 days. The experimental procedures and

* Corresponding author phone: (973)596-2477; fax: (973)596-5790; e-mail: axe@adm.njit.edu.
† Department of Civil and Environmental Engineering.
‡ Department of Physics.

10.1021/es0109848 CCC: $20.00
Published on Web 10/20/2001

TABLE 1. XAS Fits for Zn−HMO Samples Filtered over 2.4−9.2 Å^{-1} and Compared with $Zn(NO_3)_2$(aq) (*24*)[a]

Zn loadings (mol g^{-1})	T (K)	First Shell: Oxygen N (atoms)	R (Å)	σ^2 (Å^2)	C_3 (Å^3)	E_o shift (eV)
$Zn(NO_3)_2$(aq)	298	5.88 ± 0.69	2.16 ± 4.6 × 10^{-2}	1.9 × 10^{-3} ± 7.2 × 10^{-4}	5.00 × 10^{-3} ± 1.7 × 10^{-5}	3.62 ± 1.10
10^{-2} pH 7	77	6.61 ± 0.43	2.19 ± 1.3 × 10^{-2}	1.76 × 10^{-3} ± 2.6 × 10^{-4}	3.40 × 10^{-4} ± 6.0 × 10^{-5}	4.13 ± 1.42
10^{-2} pH 7	298	7.02 ± 0.24	2.19 ± 2.3 × 10^{-3}	2.43 × 10^{-3} ± 1.1 × 10^{-4}	4.50 × 10^{-4} ± 1.3 × 10^{-5}	6.79 ± 0.61
10^{-2} pH 5	298	7.07 ± 0.43	2.19 ± 3.2 × 10^{-3}	2.65 × 10^{-3} ± 2.9 × 10^{-4}	4.25 × 10^{-4} ± 1.4 × 10^{-5}	6.24 ± 0.34
10^{-2} pH 3	298	7.04 ± 0.20	2.19 ± 3.3 × 10^{-3}	2.44 × 10^{-3} ± 2.4 × 10^{-4}	3.93 × 10^{-4} ± 7.1 × 10^{-5}	6.46 ± 0.38
4 × 10^{-3} pH 7	298	7.02 ± 0.39	2.19 ± 3.2 × 10^{-3}	3.53 × 10^{-3} ± 6.1 × 10^{-4}	3.39 × 10^{-4} ± 0.9 × 10^{-5}	6.81 ± 0.54
10^{-3} pH 7[b]	77	6.80 ± 0.19	2.19 ± 3.7 × 10^{-3}	2.79 × 10^{-3} ± 8.8 × 10^{-4}	−1.58 × 10^{-4} ± 3.0 × 10^{-5}	4.81 ± 1.37
10^{-3} pH 7[c]	298	6.41 ± 0.53	2.19 ± 6.6 × 10^{-3}	3.35 × 10^{-3} ± 5.5 × 10^{-4}	9.58 × 10^{-4} ± 1.9 × 10^{-4}	7.52 ± 1.10
10^{-4} pH 7[c]	298	6.41 ± 0.35	2.19 ± 6.2 × 10^{-3}	3.35 × 10^{-3} ± 4.5 × 10^{-4}	9.58 × 10^{-4} ± 1.31 × 10^{-4}	6.29 ± 0.89

Zn loadings (mol g^{-1})	T (K)	Second Shell[d]: Oxygen N (atoms)	R (Å)	σ^2 (Å^2)	C_3 (Å^3)	% res
10^{-2} pH 7	77	8.09 ± 0.35	3.46 ± 2.3 × 10^{-2}	8.28 × 10^{-3} ± 7.2 × 10^{-4}	−1.10 × 10^{-3} ± 2.1 × 10^{-4}	6.89
10^{-2} pH 7	298	8.36 ± 0.49	3.50 ± 5.7 × 10^{-3}	9.88 × 10^{-3} ± 7.9 × 10^{-4}	−1.00 × 10^{-3} ± 1.9 × 10^{-4}	5.43
10^{-2} pH 5	298	8.10 ± 0.39	3.50 ± 1.3 × 10^{-2}	9.24 × 10^{-3} ± 5.9 × 10^{-4}	−7.79 × 10^{-4} ± 1.8 × 10^{-4}	7.61
10^{-2} pH 3	298	8.942 ± 0.92	3.50 ± 0.9 × 10^{-2}	9.60 × 10^{-3} ± 3.1 × 10^{-4}	−7.61 × 10^{-3} ± 1.7 × 10^{-4}	7.99
4 ×10^{-3} pH 7	298	8.01 ± 0.60	3.49 ± 2.2 × 10^{-2}	9.68 × 10^{-3} ± 3.0 × 10^{-4}	−1.00 × 10^{-3} ± 1.2 × 10^{-4}	7.76
10^{-3} pH 7	77	6.98 ± 0.40	3.50 ± 2.8 × 10^{-2}	1.29 × 10^{-2} ± 9.2 × 10^{-4}	−9.84 × 10^{-4} ± 2.1 × 10^{-4}	5.29

[a] *N* is the coordination number. *R* is the radial distance. σ^2 is the Debye−Waller factor. C_3 is the third-order cumulant. E_o shift is the energy shift. Errors provided with the parameters are based on standard deviations. Typically the uncertainties in *N* are estimated to be 20% for the first shell and 30% for the second shell. [b] Long-term sample analyzed after a contact time of 32 days. [c] No second shell observed; these samples were fitted over 0.5−2.2 Å. [d] Multiple shells fitted with 0.5−3.78 Å.

associated modeling results from transient studies have been discussed previously (*12*, *16*). Accordingly, Ni sorption densities after 20 and 110 days were 9.8 × 10^{-3} mol of Ni (g of HMO)$^{-1}$ (89% internal sites) and 9.9 × 10^{-3} mol of Ni (g of HMO)$^{-1}$ (90% internal sites), respectively.

The sorbed metal concentrations were measured using tracers ^{65}Zn and ^{63}Ni in duplicate studies (*12*, *16*), where the activity was measured with a Beckman LS6000SE liquid scintillation counter. Except where otherwise stated, adsorption samples were equilibrated for 4 h under turbulent hydraulic conditions ($Re \geq 3.0 \times 10^5$ with respect to the reactor length) before the solid phase was separated from the supernatant by centrifuging at 8000 rpm for 20 min. These wet pastes were loaded into aluminum or acrylic cells and sealed with Mylar windows to prevent the loss of moisture. Nickel oxide (NiO), nickel carbonate hydrate ($NiCO_3 \cdot nH_2O$), and a 1 × 10^{-3} M $Ni(NO_3)_2$ solution at pH 1 were selected as Ni references. Zn references have been studied previously and included $Zn(NO_3)_2$(aq), ZnO, $ZnO \cdot nH_2O$, and $ZnCO_3 \cdot nH_2O$ (*24*). The metal nitrate aqueous solutions were maintained at pH 1 to isolate the local structures of the hydrated metal ions.

XAS data were acquired on beamline X-11A at the National Synchrotron Light Source (NSLS), Brookhaven National Laboratory, where the electron beam energy was 2.528−2.8 GeV with a maximum beam current of 300 mA. The XAS data for the Ni−HMO adsorption samples were collected at the Ni K-edge over the energy range of 8183−9082 eV in fluorescence mode using a Lytle detector filled with Ar gas, while those for the Zn−HMO were collected at the Zn K-edge over the energy range of 9509−10408 eV under similar experimental settings. The samples were placed 45° to the incident beam. For minimizing the scattered background, the following filters were placed between one aluminum foil and the soller slits: a 3-μm Co (Z-1) filter for Ni studies and a 6-μm Cu (Z-1) filter for Zn studies. The soller slits blocked most of the filter refluorescence. Harmonic rejection was achieved by detuning the monochromator 20% of I_o. The XAS data for the reference compounds were collected over the respective K-edges in transmission mode. Prior to data collection, the energy was calibrated to the first inflection point of the metal foil standards (E_o = 8.333 keV for Ni and E_o = 9.659 keV for Zn). To elucidate the sorption mechanism at room temperature, all the adsorption samples as well as standards were studied at 298 K. Additionally, select samples were studied at 77 K to assess the thermal contributions.

The XAS spectra were analyzed using WinXAS 97 (version 1.3) following standard procedures, as recently employed in Zn adsorption to HFO and goethite (*24*). To obtain the structural information, the Fourier transforms were fit with the reference model generated using FEFF7, where all the parameters except the amplitude reduction factor (S_o^2) were allowed to float (*N* is the coordination number, *R* is the radial distance, σ^2 is the Debye−Waller factor, C_3 is the third-order cumulant, and E_o shift is the energy shift). In all cases, the maximum number of floating parameters was less than the degrees of freedom (*48*). For any given shell, a good fit was determined on the basis of the minimum residual error. A comparison of the $Ni(NO_3)_2$ solution spectra collected in transmission mode with that of the fluorescence revealed an average S_o^2 of 0.80, which was used in fitting. For all Zn samples, a S_o^2 of 0.70 was employed (*24*). In fitting multiple shells, the E_o shift was constrained to be equal. All Zn adsorption samples were fit with chalcophanite ($ZnMn_3O_7 \cdot 3H_2O$) model (*49*) generated with FEFF7 (*50*), where edge-sharing $Mn(IV)O_6$ octahedra alternate with layers of Zn ions and water molecules (*4*). All Ni samples were fitted with FEFF7-generated model for Ni_6MnO_8, an isomer of Mg_6MnO_8 where octahedrally coordinated Ni^{2+} and Mn^{4+} are located in a cubic lattice with the space group $Fm3m$ (*51*).

Results and Discussion

Standards. The local structures of Zn standards including $Zn(NO_3)_2$(aq), ZnO, $ZnO \cdot nH_2O$, and $ZnCO_3 \cdot nH_2O$ have been studied previously with XAS (*24*). These structures were consistent with their corresponding crystallographic ones (*24*). From the zinc nitrate solution (pH 1), Zn^{2+} is surrounded by approximately six oxygens at an average radial distance of 2.18 Å in a highly disordered shell (Table 1, which is taken from ref *24*). In zinc oxides, the first shell was consistent with a tetragonal structure revealing approximately four O atoms at 1.96−1.98 Å (*24*). For these oxides, a second shell of 10−12 Zn atoms at 3.21−3.24 Å was also observed (*24*).

The XAS spectra of all the Ni standards (Figure 1) show that, except for the aqueous nickel nitrate solution, second

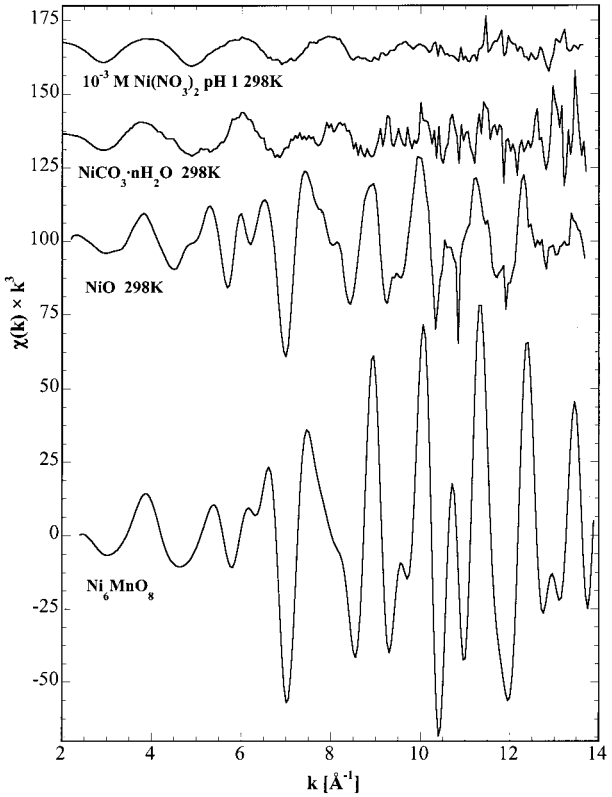

FIGURE 1. XAS spectra of Ni standards studied at 298 K and Ni K-edge in transmission mode. Ni_6MnO_8 structure is generated from crystallographic data using FEFF7 (*49*).

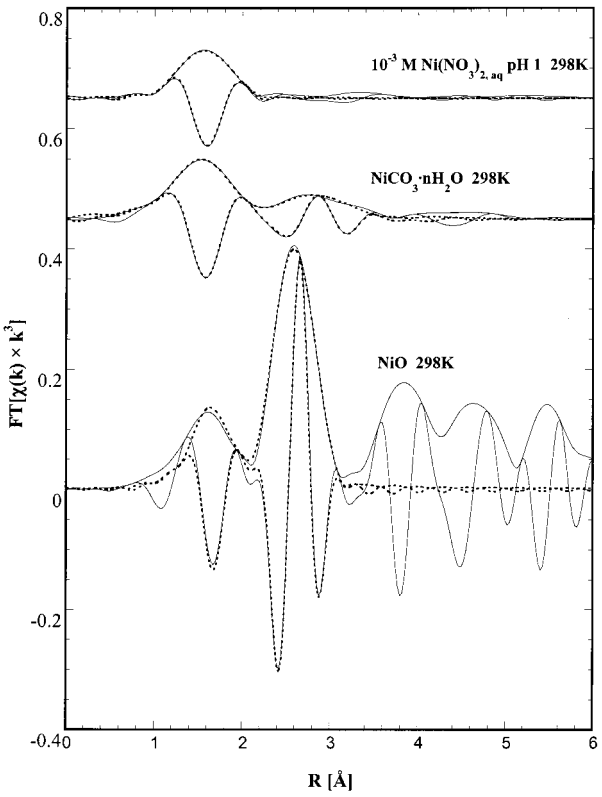

FIGURE 2. Fourier transforms (magnitude and imaginary part, solid lines) of Ni standards studied at 298 K, each filtered over *k* range of 2.4−9.22 Å^{-1} (except NiO, 2.4−13.3 Å^{-1}) and fitted with NiO (dashed lines) over 0.41−3.20 Å for NiO, 0.41−3.70 Å for $NiCO_3$·*n*H_2O, and 0.41−2.20 Å for $Ni(NO_3)_2$(aq).

shell contributions are observed. The XAS spectrum of Ni_6MnO_8 is generated from the crystallographic data using FEFF7 (*50, 51*) in which the first shell consists of two oxygens at 2.077 Å and four oxygens at 2.083 Å. The second shell is comprised of four Mn atoms at 2.421 Å and eight Ni atoms at 2.937 Å (*51*). Resultant Fourier transforms (Figure 2 and Table 2) for the Ni^{2+} ion in aqueous nickel nitrate at pH 1 and 25 °C reveal 6.08 O atoms at 2.07 Å. Thermodynamically, Ni^{2+} is the dominant species in this sample (*52*). Consistently, Magini et al. (*53*) reported the primary hydration shell radius for Ni^{2+} to be 2.07 Å. This value is based on a compilation of various experimental results including diffraction and scattering techniques, XAS, infrared and Raman spectroscopy, mass spectrometry, nuclear magnetic resonance spectroscopy, and various ab initio approaches. The fits for the Ni standards (Table 2) demonstrate that the local coordination environment is consistent with their known crystalline structures (*54*). Pandya et al. (*55*) investigated the structure of α-$Ni(OH)_2$ and found 5.8 oxygen atoms in the first shell at 2.04 Å and approximately 5.7 Ni atoms in the second shell at an average radial distance of 3.07 Å. Scheidegger et al. (*41*) presented a compilation of the structural parameters of β-$Ni(OH)_2$, $Ni(OH)_2$, and a coprecipitated phase containing Ni and Al (Ni:Al =3:1) determined using XAS, X-ray diffraction (XRD), and neutron diffraction. They found that Ni^{2+} in these three standards has an octahedral first shell coordination with R_{Ni-O} = 2.04−2.07 Å, while the second shell in nickel hydroxides was composed of 5−6 Ni atoms at 3.09−3.13 Å. A second shell was also observed in the Ni−Al coprecipitate with 3.8−4.8 Ni atoms at 3.03−3.06 Å (*41*). On the other hand, $NiCO_3$·*n*H_2O was found to have 6.74 oxygens at an average radial distance of 2.04 Å and 5.47 Ni atoms at an average distance of 3.54 Å. These results are in agreement with Pertlik (*56*), who found six O atoms in the first shell located at 2.08 Å in $NiCO_3$, while the second shell consisted of six Ni atoms at an average radial distance of 3.62 Å.

Zn−HMO Adsorption Samples. The averaged spectra for Zn sorbed to HMO (Figure 3) reveal a glitch at 10.2 Å^{-1}; this glitch is due to the presence of a fracture in the Si(111) crystal at X11A beamline. The backscattering envelopes of these spectra appear to be similar as a function of pH, adsorbate loading, and contact time, suggesting that the local coordination environment for Zn, and hence its adsorption mechanism with respect to HMO, is independent of these factors. In all of these samples, between 2.40 and 9.2 Å^{-1} the spectra show similar envelopes indicating that a light atom such as O occupies the first shell. The amplitude and the resolution of the spectra (i.e., 5.5 and 7.7 Å^{-1}) improved with increased loading. Additionally, spectra at 77 K have greater amplitudes than the corresponding ones at 298 K, revealing less thermal contributions that dampen the signal.

The Fourier transformed data show a broad distribution of 6−7 O atoms at an average radial distance of 2.19 Å (Table 2 and Figures 4−6). Application of the third-order cumulant (C_3) suggests a highly disordered oxygen shell (*32, 57, 58*). As disorder increases, additional moments of the distribution become significant; the third-order cumulant describes skewing of distribution (*32*). The structural parameters are in agreement with those for Zn^{2+} in the aqueous solution as well as with those of Zn^{2+} sorbed to HFO (*24*). The results support physical adsorption to HMO where zinc retains its waters of hydration. Beyond the first shell, in samples with higher Zn loadings and for samples with lower loadings studied at 77 K, a second shell was also observed. This shell is best fitted with 7−9 O atoms at 3.49−3.50 Å that result from functional groups on the hydrous oxide surface and/or from the hydrated interface. No meaningful fits were obtained with Zn in the second shell eliminating the possibility of precipitation or polynuclear complexation. Similarly, because of the lack of reasonable fitting parameters (e.g., $\sigma^2 < 0$ or

TABLE 2. Ni−HMO Samples and Standards[a] Fitted with NiO Model[b]

Ni loadings (mol g^{-1})	t_{rxn} (h)	*N* (atoms)	*R* (Å)	σ^2 (Å^2)	C_3 (Å^3)	E_o shift (eV)
First Shell: Oxygen						
$Ni(NO_3)_2$(aq)		6.08 ± 0.20	2.07 ± 2.0 × 10^{-3}	4.88 × 10^{-3} ± 4.3 × 10^{-4}	−6.46 × 10^{-4} ± 7.5 × 10^{-4}	3.40 ± 1.70
NiO		6.07 ± 0.32 (6)	2.06 ± 2.0 × 10^{-3} (2.08)	4.20 × 10^{-3} ± 2.8 × 10^{-4}		3.11 ± 0.42
$NiCO_3 \cdot nH_2O$		6.74 ± 0.48	2.04 ± 1.0 × 10^{-3}	9.12 × 10^{-3} ± 3.9 × 10^{-4}	−1.70 × 10^{-3} ± 7.1 × 10^{-5}	6.87 ± 1.72
10^{-2} pH 7	4	5.95 ± 0.72	2.07 ± 3.0 × 10^{-2}	5.55 × 10^{-3} ± 2.2 × 10^{-4}	−6.49 × 10^{-4} ± 2.6 × 10^{-4}	5.71 ± 0.76
10^{-2} pH 5	4	6.14 ± 0.23	2.07 ± 1.0 × 10^{-3}	5.99 × 10^{-3} ± 8.0 × 10^{-4}	−4.40 × 10^{-4} ± 1.4 × 10^{-4}	2.18 ± 1.37
8.9 × 10^{-3} pH 7	2640	5.97 ± 0.47	2.07 ± 9.0 × 10^{-2}	5.76 × 10^{-3} ± 1.2 × 10^{-4}	−4.57 × 10^{-4} ± 5.5 × 10^{-4}	6.16 ± 0.85
8.8 × 10^{-3} pH 7	480	5.92 ± 0.83	2.07 ± 1.0 × 10^{-2}	4.00 × 10^{-3} ± 1.8 × 10^{-3}	−9.00 × 10^{-4} ± 5.2 × 10^{-4}	5.57 ± 0.92
10^{-3} pH 7	4	5.75 ± 0.30	2.07 ± 1.0 × 10^{-2}	5.80 × 10^{-3} ± 1.1 × 10^{-3}	−1.00 × 10^{-4} ± 6.2 × 10^{-4}	1.32 ± 1.3
10^{-3} pH 5	4	6.17 ± 0.41	2.07 ± 4.0 × 10^{-3}	7.47 × 10^{-3} ± 6.6 × 10^{-4}	−4.45 × 10^{-4} ± 1.01 × 10^{-3}	1.45 ± 1.3

Ni loadings (mol g^{-1})	t_{rxn} (h)	*N* (atoms)	*R* (Å)	σ^2 (Å^2)	C_3 (Å^3)	% res
Second Shell: Oxygen[c]						
NiO[d]		11.31 ± 0.31 (12)	2.93 ± 1.0 × 10^{-3} (2.94)	4.22 × 10^{-3} ± 3.3 × 10^{-4}		5.87
$NiCO_3 \cdot nH_2O$[d]		5.47 ± 0.15	3.54 ± 1.0 × 10^{-3}	6.74 × 10^{-3} ± 9.9 × 10^{-4}	6.33 × 10^{-4} ± 8.1 × 10^{-5}	8.79
10^{-2} pH 7	4	5.71 ± 0.76	3.35 ± 5.0 × 10^{-2}	9.82 × 10^{-3} ± 3.7 × 10^{-4}	−8.79 × 10^{-3} ± 1.4 × 10^{-3}	8.84
10^{-2} pH 5	4	8.36 ± 0.49	3.35 ± 2.0 × 10^{-2}	9.70 × 10^{-3} ± 4.1 × 10^{-4}	−8.15 × 10^{-3} ± 1.7 × 10^{-3}	7.54
8.9 × 10^{-3} pH 7	2640	6.16 ± 0.85	3.34 ± 3.0 × 10^{-2}	9.00 × 10^{-3} ± 1.8 × 10^{-3}	−4.59 × 10^{-3} ± 1.0 × 10^{-3}	5.24
8.8 × 10^{-3} pH 7	480	5.57 ± 0.92	3.32 ± 9.0 × 10^{-2}	8.36 × 10^{-3} ± 2.3 × 10^{-3}	−5.40 × 10^{-3} ± 5.9 × 10^{-4}	5.01
10^{-3} pH 7	4	6.30 ± 0.94	3.34 ± 2.0 × 10^{-2}	9.90 × 10^{-3} ± 2.2 × 10^{-3}	−6.50 × 10^{-4} ± 5.1 × 10^{-4}	4.92
10^{-3} pH 5	4	6.21 ± 0.83	3.35 ± 1.0 × 10^{-2}	9.71 × 10^{-3} ± 4.2 × 10^{-4}	−2.83 × 10^{-4} ± 1.3 × 10^{-3}	9.04

[a] Ni standards filtered over 2.40−9.2 Å^{-1}, except for NiO, 2.40−13.33 Å^{-1}. NiO fitted over 0.41−3.20 Å, $NiCO_3$ fitted over 0.4−3.70 Å, and aqueous $Ni(NO_3)_2$ fitted over 0.4−2.20 Å. [b] Errors provided with the parameters are based on the standard deviations. Typically the uncertainties in *N* are estimated to be 20% for the first shell and 30% for the second shell. All samples were Fourier transformed from 2.45 to 9.21 Å^{-1} and fitted for multiple shells over 0.5−3.78 Å. Numbers in parentheses correspond to parameters determined from XRD. [c] Oxygen contributions in the second shell were observed only in Ni−HMO adsorption samples. [d] Second shell contributions in Ni standards are from Ni atoms only.

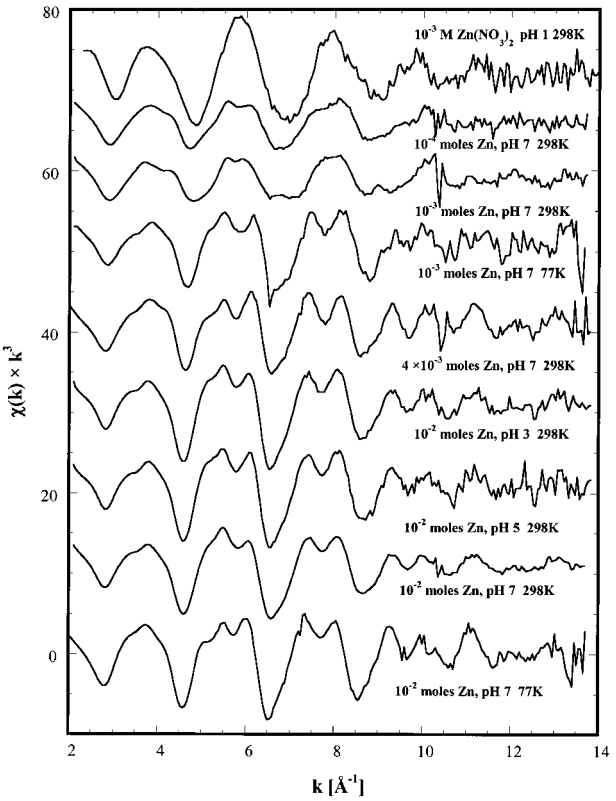

FIGURE 3. XAS spectra of Zn−HMO adsorption samples studied at Zn K-edge in fluorescence mode as a function of pH, adsorbate loading, temperature, and contact time as compared with that of $Zn(NO_3)_2$(aq) collected in transmission mode at 298 K.

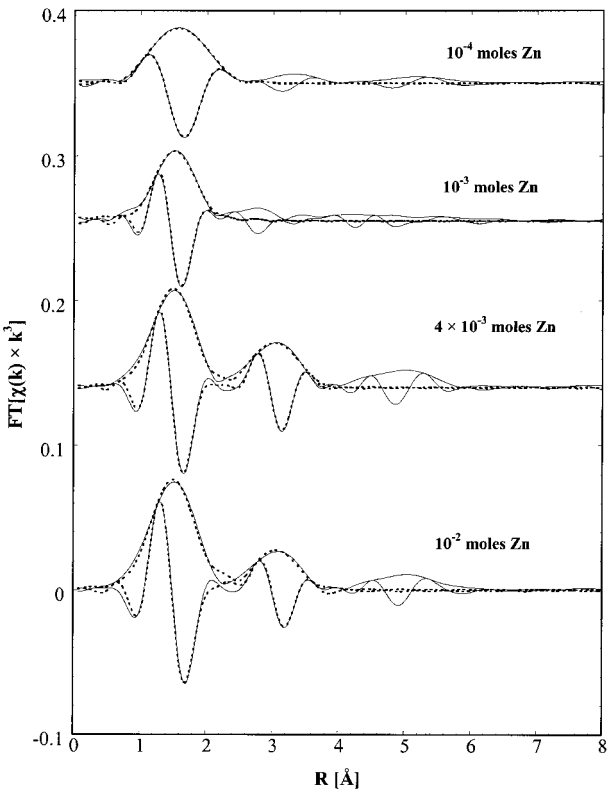

FIGURE 4. Fourier transforms (magnitude and imaginary part, solid lines) of XAS spectra of Zn−HMO adsorption samples at pH 7 and 298 K, presented as a function of Zn concentration and reaction time, each filtered over *k* range of 2.4−9.4 Å^{-1} and fitted with chalcophanite (dashed lines) over 0.5−3.78 Å (except single shells over 0.5−2.2 Å).

$N > 200$) for fitting Mn in the second shell, no Zn−Mn pairing could be identified in this second shell, further supporting the hypothesis of physical adsorption (*12*, *16*). Temperature dependence (Table 2 and Figure 6) also confirms physical forces due to a significant contribution from the thermal component of the Debye−Waller factor. Given the errors of at least ±20% associated with these coordination numbers,

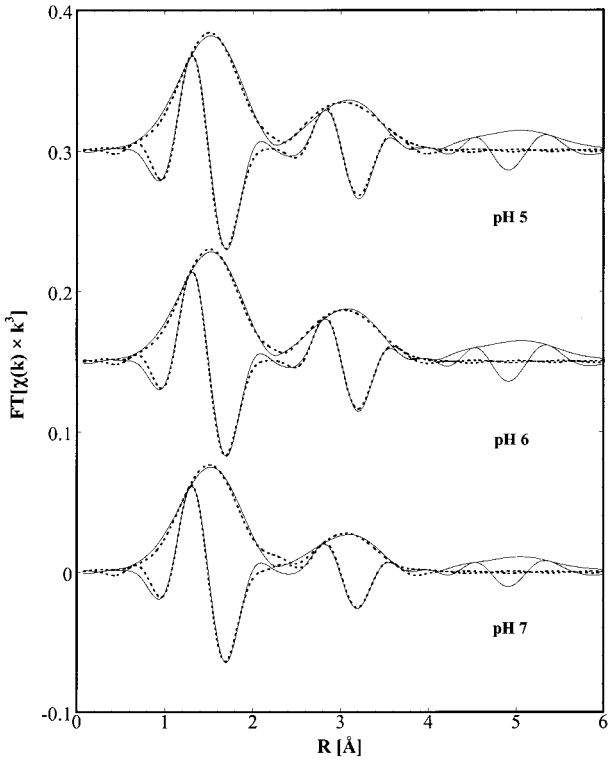

FIGURE 5. Fourier transforms (magnitude and imaginary part, solid lines) of XAS spectra of Zn−HMO adsorption samples at 298 K, presented as a function of pH, each filtered over *k* range of 2.4−9.4 Å^{-1} and fitted with chalcophanite (dashed lines) over 0.5−3.78 Å (except single shells over 0.5−2.2 Å).

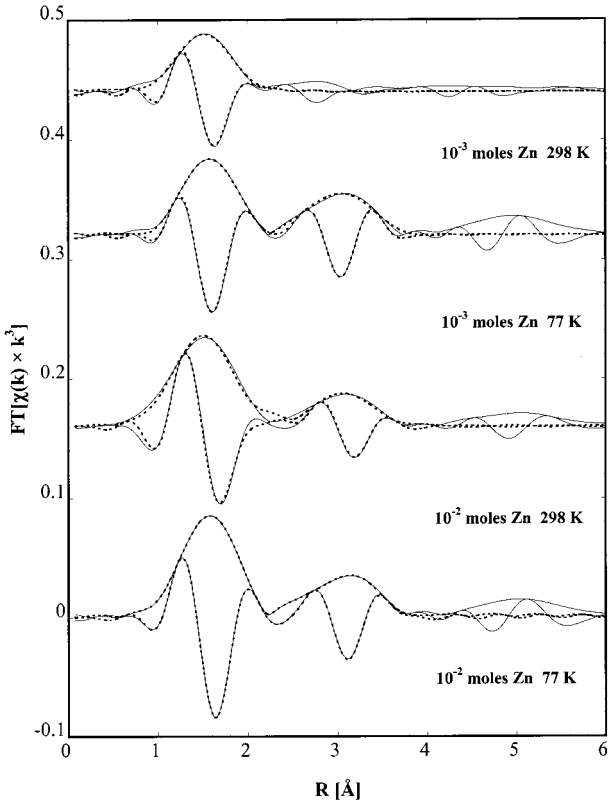

FIGURE 6. Fourier transforms (magnitude and imaginary part, solid lines) of XAS spectra of Zn−HMO adsorption samples at pH 7, presented as a function of temperature, each filtered over *k* range of 2.4−9.4 Å^{-1} and fitted with chalcophanite (dashed lines) over 0.5−3.78 Å (except single shells over 0.5−2.2 Å).

the local structure is independent of adsorbate concentration (Figure 4) and of pH (Figure 5), indicating that Zn adsorption to HMO can be represented by one average mechanism. This result complements the macroscopic studies (*12*) where linear isotherms suggested one average type of site and enthalpies were indicative of physical adsorption. Interestingly, the local structure of the long-term sample (t = 32 days) with an adsorbate loading of 4×10^{-3} mol of Zn (g of HMO)$^{-1}$ (Figure 4) is similar to that of the 4-h sample. Because the data represent a volume average where approximately 33% of the Zn is located internally, when Zn diffuses along the micropore walls of HMO, its sorption mechanism is similar to that on the external surface (4-h sample) (*12*). Axe and co-workers (*32, 33*) have further demonstrated from their spectroscopic studies with Sr−HFO and Sr−HMO systems that the local structure of Fe in HFO and of Mn in HMO did not change in the presence of Sr for up to 6 months.

In contrast to this work, other studies report the transition of the 6-fold coordination of Zn ions to a 4-fold one upon sorption to ferrihydrite (*46*), to goethite (*24*), to α-alumina powders at low sorption densities (*47*), and in zinc−ferric hydroxide coprecipitation (*59*). At higher sorption densities, although Trainor et al. (*47*) observed six O atoms in the first shell at approximately 2.02 Å, they surmised that two atoms were from the alumina surface. Furthermore, they concluded that at low sorption concentrations, Zn ions formed predominantly an inner-sphere bidentate complex with AlO_6 polyhedra, whereas at higher sorption densities Zn formed a mixed metal hydroxide coprecipitate (*47*). XAFS studies of Zn sorption to pyrophyllite as a function of surface loading (0.1−1.6 μmol m^{-2} pyrophyllite) and time revealed the formation of Zn−Al LDH where the crystalline stability increased with aging (*45*). On the other hand, Schlegel et al. (*23*) observed that Zn ions in a nitrate solution as well as in a complex with EDTA retained the octahedral hydration shell upon sorption to goethite.

Results from macroscopic studies suggest that a group of metals from the Periodic Table form similar adsorption complexes (*12, 16*). To test this hypothesis, Ni sorption to HMO was evaluated.

Ni−HMO Adsorption Samples. The local structure of Ni sorbed to HMO as a function of pH, adsorbate concentration, and reaction time suggests that the adsorption mechanism is independent of these parameters (Figure 7). The spectra reveal two backscattering envelopes indicative of two shells. The amplitude and the signal-to-noise ratio of these spectra improved with the adsorbate loading. Fits showed (Table 2 and Figures 8 and 9) 5.8−6.2 O atoms in a highly disordered first shell at an average distance of 2.07 Å. The first shell parameters are similar to those of the aqueous Ni ion, suggesting that the primary hydration shell remains intact upon sorption. Scheidegger et al. (*40*) reported six oxygens at 2.02-2.04 Å around Ni sorbed to pyrophyllite at all sorption densities up to 2.99×10^{-4} mol g^{-1}. Roberts et al. (*60*) observed a first shell coordination of 5.4−6.9 O atoms at 2.05−2.06 Å for Ni sorbed to a soil clay fraction; they found this shell to be independent of pH and contact time.

Second shell contributions were best represented with 5.6−8.4 oxygen atoms ranging from 3.32 to 3.35 Å (Table 2 and Figure 8). Surface precipitation, polymerization, or coprecipitation is excluded since there was no evidence of Ni in the second shell. Similarly, no plausible fits were obtained with Mn atoms in the second shell. Thus, Ni sorption to HMO is best described as an outer-sphere mechanism, which is independent of pH and adsorbate concentration (*16*). Furthermore, results (Figure 9 and Table 2) show that the local structure of Ni did not change between 4 h and 110

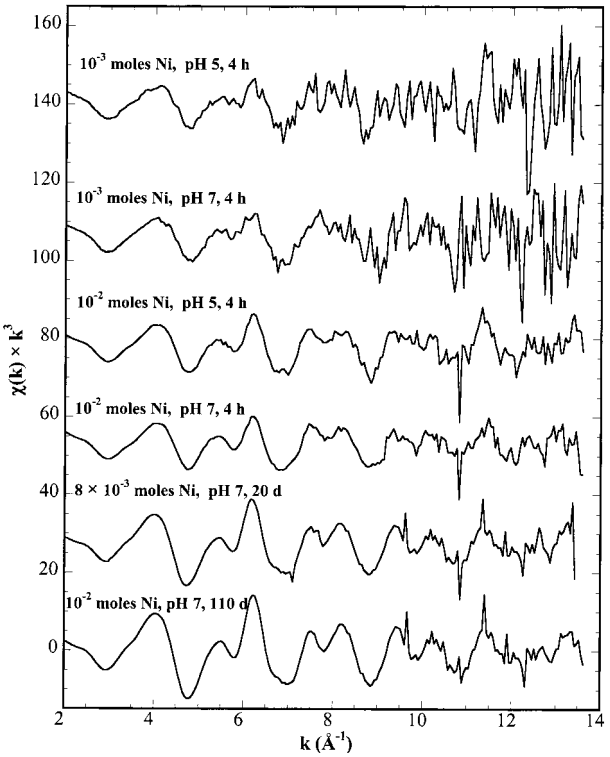

FIGURE 7. XAS spectra of Ni sorbed to HMO studied at 298 K and Ni K-edge in fluorescence mode as a function of pH, adsorbate loading, and contact time.

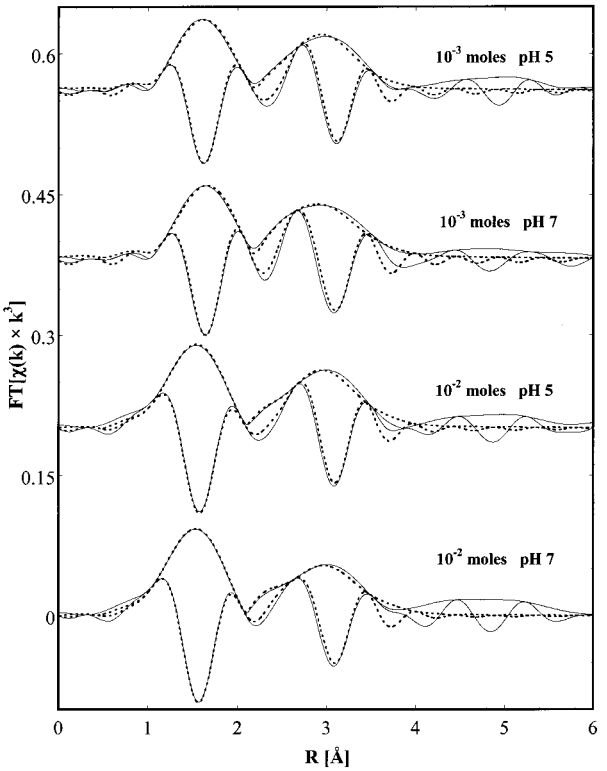

FIGURE 8. Fourier transforms (magnitude and imaginary part, solid lines) of Ni K-edge XAS spectra of Ni sorbed to HMO studied at 298 K presented as a function of pH and adsorbate concentration, each filtered over *k* range of 2.45−9.21 Å^{-1} and fitted with Ni_6MnO_8 (dashed lines) over 0.41−4.00 Å.

days during which the amount of Ni sorbed increased from 10^{-3} to 10^{-2} mol (g of HMO)$^{-1}$. In this latter case, however, as much as 90% of Ni sorbed was associated with surface

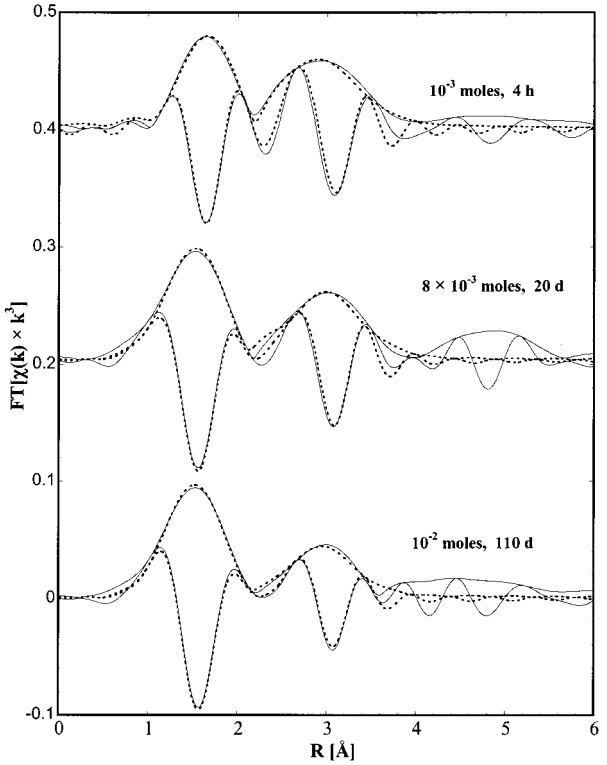

FIGURE 9. Fourier transforms (magnitude and imaginary part, solid lines) of XAS spectra of Ni sorbed to HMO studied at pH 7 and 298 K, presented as a function of contact time, each filtered over *k* range of 2.45−9.21 Å^{-1} and fitted with Ni_6MnO_8 (dashed lines) over 0.41−4.00 Å.

sites located along the micropore walls; further supporting that internal sites are equivalent to external ones. Thus, similar to Zn, Ni sorption to microporous oxides such as HMO is most appropriately explained by intraparticle surface diffusion as recently observed in macroscopic studies (*16*). Other works (*31*−*33, 38, 39*) provide spectroscopic evidence of intraparticle diffusion in microporous oxides as well. On the other hand, as mentioned earlier, Sparks and co-workers (*40*−*44*) have found from extensive kinetic studies of Ni sorption to clay surfaces that Ni forms a Ni−Al LDH. In such precipitates, the second shell is generally a result of contributions from Ni at 3.05−3.06 Å and from Al at 3.06−3.12 Å with Ni/Al coordination ratios ranging from 1 to 3 depending upon the initial conditions (*40*−*44*).

The striking similarity in the local structures of Ni^{2+} and Zn^{2+} sorbed to HMO as a function of pH, adsorbate concentration, and reaction time corroborates that a group of metals from the Periodic Table form similar adsorption complexes with HMO and possibly other hydrous amorphous oxides such as that of Al and Fe. A comparison of Sr sorption to HMO with that of Ni and Zn demonstrates the higher affinity transition metals have for the oxide surface over alkaline earth metals. Furthermore, this research supports the importance of including intraparticle diffusion in the modeling contaminant mobility and bioavailability.

Acknowledgments

This research was funded through NSF Grants BES-9753072 and BES-0089903, start-up funds granted to L.A. from the New Jersey Institute of Technology and the DuPont Young Professor's and Aid to Education Grants. The authors thank James Dyer of DuPont Engineering Technology for his input and support. The authors also acknowledge the technical support of staff at the X11A beamline in NSLS at Brookhaven National Laboratory.

Literature Cited

(1) Jenne, E. A. In *Trace Inorganics in Water*; Gould, R. F., Ed.; ACS Advances in Chemistry 73; American Chemical Society: Washington, DC, 1968; pp 337−387.
(2) McKenzie, R. M. In *Minerals in Soil Environment*; Dixon, J. B., Weed, S. B., Eds.; Soil Society of America Book Series 1; Soil Society of America: Madison, WI, 1989; pp 438−471.
(3) Fritsch, S.; Post, J. E.; Navrotsky, A. *Geochim. Cosmochim. Acta* **1997**, *61*, 2613−2616.
(4) Post, J. E. *Proc. Natl. Acad. Sci. U.S.A.* **1999**, *96*, 3447−3454.
(5) Manceau, A.; Combes, J. M. *Phys. Chem. Miner.* **1988**, *15*, 283−295.
(6) Manceau, A.; Gorshkov, A. I.; Drits, V. A. *Am. Mineral.* **1992**, *77*, 1133−1143.
(7) Manceau, A.; Gorshkov, A. I.; Drits, V. A. *Am. Mineral.* **1992**, *77*, 1144−1157.
(8) McKenzie, R. M. *Aust. J. Soil. Res.* **1980**, *18*, 61−73.
(9) Tamura, H.; Katayama, N.; Furuichi, R. *Environ. Sci. Technol.* **1996**, *30*, 1198−1204.
(10) Pedersen-Green, H.; Jensen, B. T.; Pind, N. *Environ. Technol.* **1997**, *18*, 807−815.
(11) Trivedi, P.; Axe, L. *J. Colloid Interface Sci.* **1999**, *218*, 554−563.
(12) Trivedi, P.; Axe, L. *Environ. Sci. Technol.* **2000**, *34*, 2215−2223.
(13) Bartlett, R.; James, B. *J. Environ. Qual.* 1990, *8* (1), 31−35.
(14) Huang, P. M. In *Rates of Soil Chemistry Processes*; Sparks, D. L., Suarez, D. L., Eds.; Soil Science Society of America: Madison, WI, 1989; pp 191−230.
(15) Scott, M. J.; Morgan, J. J. *Environ. Sci. Technol.* **1996**, *30*, 1990−1996.
(16) Trivedi, P.; Axe, L. *Environ. Sci. Technol.* **2001**, *35*, 1779−1784.
(17) Charlet, L.; Manceau, A. A. *J. Colloid Interface Sci.* **1992**, *148* (2), 443−458.
(18) Manceau, A.; Charlet, L. *J. Colloid Interface Sci.* **1992**, *148*, 425−442.
(19) Spadini, L.; Manceau, A.; Schindler, P. W.; Charlet, L. *J. Colloid Interface Sci.* **1994**, *168*, 73−86.
(20) Manceau, A.; Charlet, L. *J. Colloid Interface Sci.* **1994**, *168* (1), 87−93.
(21) Waite, T. D.; Davis, J. A.; Payne, T. E.; Waychunas, G. A.; Xu, N. *Geochim. Cosmochim. Acta* **1994**, *58* (24), 5465−5478.
(22) Fendorf, S.; Eick, M. J.; Grossl, P.; Sparks, D. L. *Environ. Sci. Technol.* **1997**, *31* (2), 315−320.
(23) Schlegel, M. L.; Manceau, A.; Charlet, L. *J. Phys. IV Fr.* 7 **1997**, 823−824.
(24) Trivedi, P.; Axe, L.; Tyson, T. *J. Colloid Interface Sci.*, in press.
(25) Bargar, J. R.; Brown, G. E., Jr.; Parks, G. A. *Geochim. Cosmochim. Acta* **1997**, *61* (13), 2639−2652.
(26) Bargar, J. R.; Brown, G. E., Jr.; Parks, G. A. *Geochim. Cosmochim. Acta* **1998**, *62* (2), 193−207.
(27) Weesner, F. J.; Bleam, W. F. *J. Colloid Interface Sci.* **1998**, *205*, 380−389.
(28) Bargar, J. R.; Brown, G. E., Jr.; Parks, G. A. *Geochim. Cosmochim. Acta* **1997**, *61*, 2617−2637.
(29) Chisholm-Brause, C. J.; Hayes, K. F.; Roe, A. L.; Brown, G. E., Jr.; Parks, G. A.; Leckie, J. O. *Geochim. Cosmochim. Acta* **1990**, *54*, 1897−1909.
(30) Collins, C. R.; Sherman, D. M.; Ragnarsdottir, K. V. *J. Colloid Interface Sci.* **1999**, *219*, 345−350.
(31) Scheinost, A. C.; Abend, S.; Pandya, K. I.; Sparks, D. L. *Environ. Sci. Technol.* **2001**, *35* (6), 1090−1096.
(32) Axe. L.; Bunker, G.; Anderson, P. R.; Tyson, T. *J. Colloid Interface Sci.* **1998**, *199*, 44−52.
(33) Axe. L.; Tyson, T.; Trivedi, P.; Morrison, T. *J. Colloid Interface Sci.* **2000**, *224*, 408−416.
(34) Sahai, N.; Carroll, S. A.; Roberts, S.; O'Day, P. A. *J. Colloid Interface Sci.* **2000**, *222*, 198−212
(35) Bargar, J. R.; Persson, P.; Brown, G. E., Jr. *Geochim. Cosmochim. Acta* **1999**, *63*, 2957−2969.
(36) Manceau, A.; Charlet, L.; Boisset, M. C.; Didier, B.; Spadini, L. *Appl. Clay Sci.* **1992**, *7* (1−3), 201−223.
(37) Fendorf, S.; Jardine, P. P.; Patterson, R. R.; Taylor, D. L.; Brooks, S. C. *Geochim. Cosmochim. Acta* **1999**, *63* (19/20), 3049−3057.
(38) Waychunas, G. A.; Rea, B. A.; Fuller, C. C.; David, J. A. *Geochim. Cosmochim. Acta* **1993**, *57*, 2251−2269.
(39) Papelis, C.; Brown, G. E., Jr.; Parks, G. A.; Leckie, J. O. *Langmuir* **1995**, *11* (6), 2041−2049.
(40) Scheidegger, A. M.; Lamble, G. M.; Sparks, D. L. *Environ. Sci. Technol.* **1996**, *30* (2), 548−554.
(41) Scheidegger, A. M.; Strawn, D. G.; Lamble, G. M.; Sparks, D. L. *Geochim. Cosmochim. Acta* **1998**, *62* (13), 2233−2245.
(42) Ford, R. G.; Scheinost, A. C.; Scheckel, K. G.; Sparks, D. L. *Environ. Sci. Technol.* **1999**, *33*, 3140−3144.
(43) Scheinost, A. C.; Ford, R. G.; Sparks, D. L. *Geochim. Cosmochim. Acta* **1999**, *63* (19/20), 3193−3203.
(44) Elzinga, E. J.; Sparks, D. L. *J. Colloid Interface Sci.* **1999**, *213*, 506−512.
(45) Ford, R. G.; Sparks, D. L. *Environ. Sci. Technol.* **2000**, *34*, 2479−2483.
(46) Waychunas, G. A.; Fuller, C. C.; Davis, J. A. In *1994 Activity Report*; Stanford Synchrotron Radiation Laboratory: 1995; pp 78−80.
(47) Trainor, T. P.; Brown, G. E., Jr.; Parks, G. A. *J. Colloid Interface Sci.* **2000**, *231*, 359−372.
(48) Stern, E. A. *Phys. Rev. B* **1993**, *48*, 9825−9827.
(49) Post, J. E.; Appleman, D. E. *Am. Mineral.* **1988**, *73*, 1401−1404.
(50) Zabinsky, S. I.; Reher, J. J.; Ankudinov, A.; Albers, R. C.; Eller, M. J. *Phys. Rev. B* **1995**, *52*, 2995.
(51) Porta, P.; Minelli, G.; Botto, I. L.; Baran, E. J. *J. Solid State Chem.* **1991**, *92*, 202−207.
(52) Allison, J. D.; Brown D. S.; Novo-Gradac, K. J. *MINTEQA2/PRODEFA2: A Geochemical Assessment Model for Environmental Systems*; Center for Exposure Assessment Modeling, U.S. EPA: 1991.
(53) Magini, M.; Licheri, G.; Paschina, G.; Piccaluga, Pinna, G. *X-ray Diffraction of Ions in Aqueous Solutions: Hydration and Complex Formation*; CRC Press Inc.: Boca Raton, FL, 1988.
(54) Wyckoff, R. W. G. *Crystal Structures: Vol. 1*, 2nd ed.; John Wiley & Sons: New York, 1963.
(55) Pandya, K. I.; O'Grady, W. E.; Corrigan, D. A.; McBreen, J.; Hoffman, R. W. *J. Phys. Chem.* **1990**, *94*, 21−26.
(56) Pertlik, F. *Acta Crystallogr.* **1985**, *156*, 177−186.
(57) Bunker, G. *Nucl. Instrum. Methods* **1983**, *207*, 237−243.
(58) Bunker, B.; Sayers, D. In *X-ray Absorption: Principles, Applications, Techniques of EXAFS, SEXAFS, and XAFS*; Koningsberger, D. C., Prins, R., Eds.; Wiley: New York, 1988.
(59) O'Day, P. A.; Carroll, S. A.; Waychunas, G. A. *Environ. Sci. Technol.* **1998**, *32*, 943−955.
(60) Roberts, D. R.; Scheidegger, A. M.; Sparks, D. L. *Environ. Sci. Technol.* **1999**, *33*, 3749−3754.

Received for review May 17, 2001. Revised manuscript received September 10, 2001. Accepted September 18, 2001.

ES0109848